Highlights from Muon Scattering at CERN

Rüdiger Voss
CERN, CH–1211 Geneva 23, Switzerland

Abstract

A review is given of recent results from the deep inelastic muon scattering program at CERN, focusing on high statistics measurements of scaling violations and tests of QCD, and on past and future experiments to measure the spin structure functions of the nucleon.

1 Introduction

A vigorous experimental programme on deep inelastic muon scattering has been underway at the CERN SPS since 1978, and is still going strong. Two large detector systems have been built to carry out this programme. The European Muon Collaboration (EMC) has built a versatile spectrometer system designed around a large aperture dipole magnet [1] which has produced a wealth of results covering almost all aspects of high energy muon scattering. Important discoveries have been made with this apparatus, notably the first measurement of nuclear effects in deep inelastic scattering and the surprising results on the so-called "spin crisis" of the proton. Many of the EMC measurements of nucleon structure functions have been repeated by the New Muon Collaboration (NMC) with an upgraded version of the same spectrometer, with improved systematic accuracy and covering an enlarged kinematical region. The analysis of most of the NMC data is still underway. Finally, the Spin Muon Collaboration (SMC) has embarked since 1991 on a comprehensive programme to measure the spin structure functions of the nucleon, using yet another upgrade of the EMC spectrometer, a large polarized target, and a newly designed beam polarimeter.

The BCDMS Collaboration (Bologna-CERN-Dubna-Munich-Saclay, 1978–1985) has opted for a very different experimental approach to high energy muon scattering and built a detector based on a very long (50 m) toroidal iron magnet, enclosing an almost equally long target [2]. By its design, the physics scope of this apparatus was essentially limited to the study of inclusive muon scattering, and to a somewhat smaller kinematic range. The kinematic acceptance of this apparatus has subsequently been enlarged at the expense of sacrifying a part of the luminosity. Still, the enormous length of the target allowed for a much higher statistical accuracy than could be achieved with the EMC apparatus. Best known

Table 1: Physics issues addressed by the CERN muon experiments

Collaboration Data taking	BCDMS 1978–85	EMC 1978–85	NMC 1986–89	SMC 1991–
F_2, $R = \sigma_L/\sigma_T$	X	X	X	
QCD studies, measurements of α_s	X	X	X	
Nuclear effects	X	X	X	
Spin structure functions		X		X
Hadronic final states		X		
Electroweak interference	X			

among the BCDMS results are the high statistics measurements of the structure functions $F_2(x,Q^2)$ and $R = \sigma_L/\sigma_T$ on proton, deuterium, and carbon targets, and the unique measurement of weak-electromagnetic interference effects in deep inelastic muon-carbon scattering. An overview over the CERN muon experiments and the main physics issues which they address is given in Table 1.

All these experiments have shared the same muon beam M2 of the CERN Super Proton Sychrotron (SPS). Most data were taken at beam energies between 90 and 280 GeV. The beam has recently been upgraded to improve its optical properties for the critical requirements of the SMC experiment, at the expense of reducing the maximum energy from 280 to 200 GeV.

The present review focuses on the BCDMS data on $F_2(x,Q^2)$ obtained with hydrogen and deuterium targets, especially on the study of scaling violations, and on the EMC results on the proton spin structure function $g_1(x)$. All these data nicely complement earlier measurements with the SLAC electron beam at lower energies. A complete review of earlier CERN results can be found in [3]. The phenomenology of deep inelastic scattering has been introduced by earlier speakers at this school and I will not repeat it here, with the exception of deep inelastic scattering of polarized muons on polarized targets for which I will discuss the formalism in some detail.

2 High statistics results on nucleon structure functions

2.1 Recent measurements of $F_2(x,Q^2)$

The experimental situation of the structure function F_2 measured on light targets (hydrogen and deuterium) has somewhat confused since the publication of the BCDMS data [4, 5] which are in disagreement with earlier data from the EMC [6, 7] (Fig. 1). The x dependences of $F_2(x,Q^2)$ measured by these two experiments are different outside the published systematic uncertainties. Note, however, that this discrepancy has often been overestimated and overemphasized due to a neglect of correlation effects in the systematic errors which are important in these experiments in the region of large x [8].

Several new results have recently become available which clarify most of this confusion. The SLAC E-140 group has undertaken a comprehensive and coherent reanalysis of a series of electron scattering experiments performed at SLAC between 1970 and 1985 on hydrogen and deuterium targets, with the aim of extracting a single authoritative set of data on the structure functions F_2 and $R = \sigma_L/\sigma_T$ with reduced statistical and systematic errors [9]. The results of this analysis are also shown in Fig. 1. An unambigous comparison between the electron and the muon data is difficult since they cover almost disjoint domains of Q^2, but two independent analyses [8, 9] come to the same conclusion that, in order to optimize the overall agreement between the three experiments, the BCDMS data should be renormalized downwards by 2% or less and the EMC data upwards by $\approx 8\%$ when the SLAC data are used as an arbitrary reference. Such a manipulation brings all three experiments in good mutual agreement in the region of Q^2 overlap at large x, and also at smaller x when comparing electron and muon data via a physically meaningful Q^2 evolution procedure [8]. The heuristic renormalization factors are in acceptable agreement with the quoted normalization uncertainties of 2%, 3% and 5% for the SLAC, BCDMS and EMC data, respectively. Applying overall normalization factors to the data does, of course, not resolve the problem of different x dependences.

Two more results have recently become available which are more directly comparable to the EMC and BCDMS data. Preliminary data from the NMC on hydrogen and deuterium targets [10], measured at beam energies of 90 and 280 GeV, also indicate excellent agreement with the earlier BCDMS results; as an example, the deuterium data are shown in Fig. 2. This figure also shows that the NMC has made substantial progress in extending the kinematic range of these measurements to much smaller values of x.

Finally, the Fermilab CCFR Collaboration has recently presented their high statistics results on the structure functions F_2^ν and xF_3^ν from deep inelastic neutrino interactions on iron. After correcting for the quark charges, and after small corrections for non-isoscalarity and nuclear effects, these data also show good agreement with the BCDMS results [11].

A more quantitative comparison between these experiments will have to wait for the NMC and CCFR results to become available in their final numerical form. Nevertheless it seems fair to conclude that all recent data are in good agreement with the BCDMS results, i.e., favour a "large" F_2 at small x and a steeper x dependence when compared to the earlier EMC data.

2.2 Scaling violations and tests of perturbative QCD

Deep inelastic scattering continues to be one of the most fruitful grounds to test predictions of perturbative QCD and to measure the strong coupling constant α_s. The subject has been introduced at this school by T. Hansl [12] and I do not

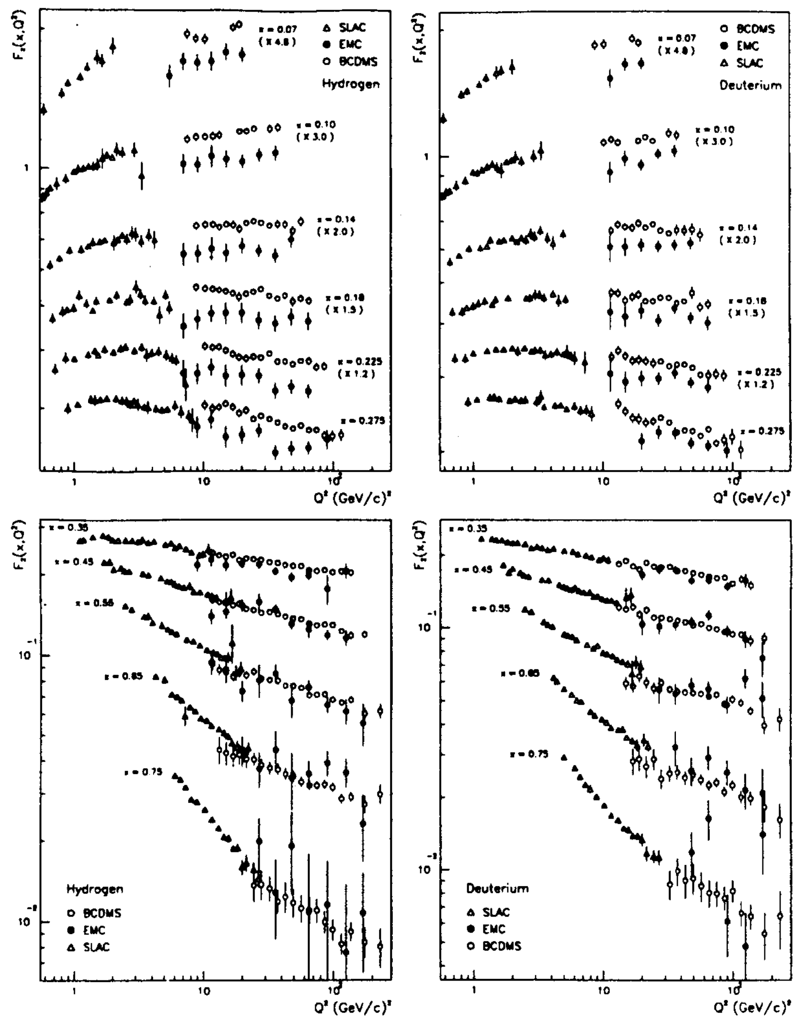

Figure 1: The structure function $F_2(x, Q^2)$ measured by the SLAC, EMC, and BCDMS experiments on hydrogen (left) and deuterium (right) targets. The error bars show statistical and systematic errors combined in quadrature. The EMC data are interpolated to the SLAC/BCDMS bins of x. All Data are shown for the assumption that $R = R_{QCD}$.

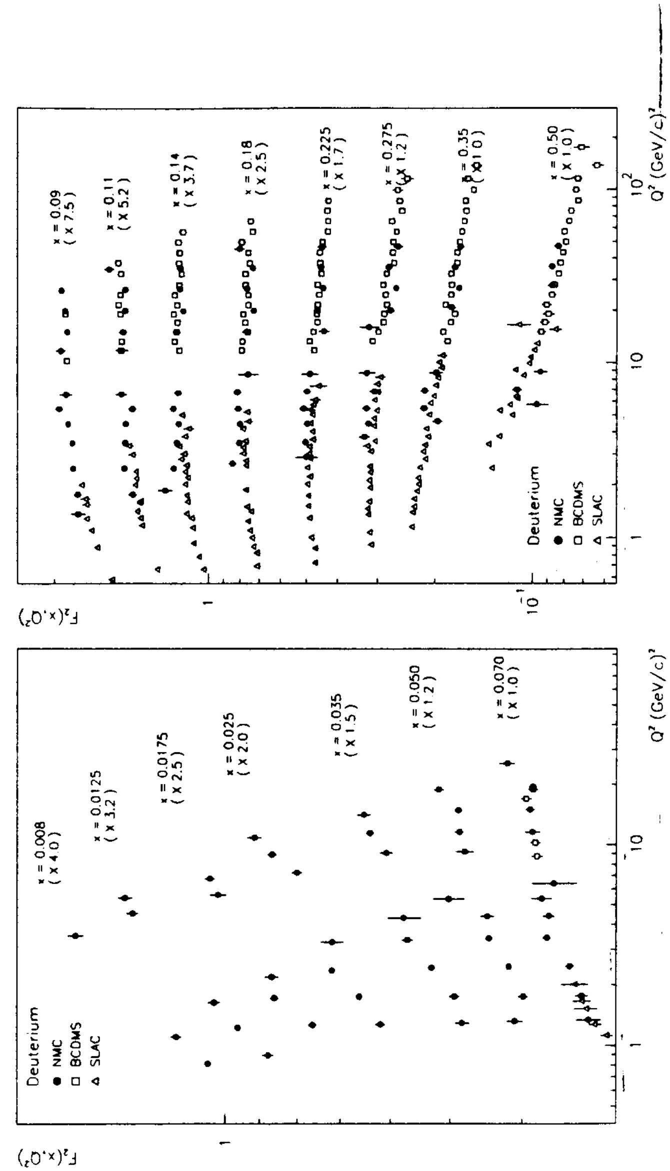

Figure 2: The structure function $F_2(x, Q^2)$ measured by the NMC experiment on a deuterium target, compared to earlier results from BCDMS and SLAC. All Data are shown for the assumption that $R = R_{QCD}$.

need to discuss here the theoretical foundations of such tests. The experimental knowledge of scaling violations has improved significantly over the last years with the advent of high statistics data from free or quasifree nucleon targets (hydrogen and deuterium) which are free of ambiguities from nuclear effects. The most extensive QCD studies so far have been based on the BCDMS data shown in Fig. 1. The observed scaling violations, more precisely the measured logarithmic derivatives $d\ln F_2/d\ln Q^2$, can be directly compared to perturbative QCD predictions by virtue of the Altarelli-Parisi equations [13]. This is shown in Fig. 3 where good agreement is observed with such predictions computed in next-to-leading order, for the example of the BCDMS deuterium data [5]. In a flavour nonsinglet approximation at $x > 0.25$ where the influence of the gluon distribution can be safely neglected, the fit gives for the QCD mass scale parameter

$$\Lambda^{(4)}_{\overline{MS}} = 230 \pm 40\,(\text{stat.}) \pm 70\,(\text{syst.})\,\text{MeV},$$

where the superscript refers to the number of quark flavours assumed in the analysis. This is in good agreement with an earlier result from the same group obtained with hydrogen and carbon target data [14, 15],

$$\Lambda^{(4)}_{\overline{MS}} = 220 \pm 15\,(\text{stat.}) \pm 50\,(\text{syst.})\,\text{MeV}.$$

In all cases, a combined flavour singlet and nonsinglet analysis covering the full x range of the data gives a similar result. Together with the recent CCFR results from neutrino scattering, these are the most precise and reliable data Λ_{QCD} from an individual deep inelastic experiment which are available today.

The combined SLAC and BCDMS data can be used for QCD fits over an extended range in Q^2; a very careful study has recently been presented by Virchaux and Milsztajn [16]. Perturbative QCD is not expected to hold down to the lowest Q^2 values of the SLAC data ($Q^2 \approx 1$ GeV^2) and these fits therefore include dynamical twist-four coefficients C_i describing the Q^2 evolution of F_2 in the low Q^2 regime due to nonperturbative effects:

$$F_2^{HT}(x_i, Q^2) = F_2^{LT}(x_i, Q^2)(1 + C_i/Q^2), \tag{1}$$

where F_2^{LT} is the leading twist structure function assumed to follow the Altarelli-Parisi equations. The coefficients C_i are fitted separately in each bin of x and the data are corrected for target mass effects. The relative normalisation between the two experiments is included as a free parameter in the fit. Furthermore, the BCDMS data are allowed to vary according to dominant systematic uncertainties in the region of large x, to account for small residual discrepancies in the Q^2 overlap region around $Q^2 \approx 20$ GeV^2 (Fig. 1). These systematic errors originate mostly from uncertainties in the momentum calibrations of the BCDMS experiment. They are are fully correlated and can be described by a single parameter which is included in the fit. Target mass corrections are also included [17].

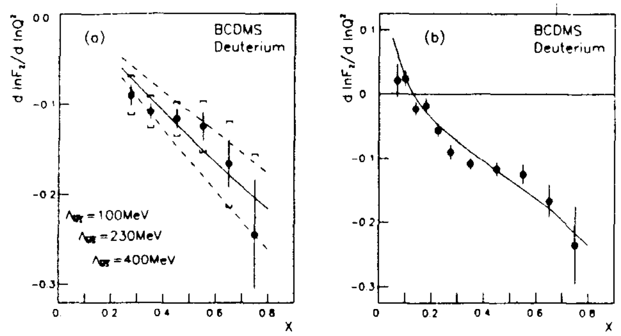

Figure 3: (a) The logarithmic derivatives $d\ln F_2/d\ln Q^2$ measured by BCDMS on a deuterium target, averaged over Q^2, for $Q^2 > 20$ GeV^2 and $x \geq 0.275$. The inner error bars are statistical, the outer error bars statistical and systematic errors added linearly. The lines show QCD predictions for different values of Λ. (b) The same as (a), over the full x range of the data. The solid line is the result of the QCD fit discussed in the text.

The results of a next-to-leading order fit can be summarised as follows. The BCDMS hydrogen data should be renormalized by -1%; no renormalization is required for the deuterium data. The BCDMS hydrogen (deuterium) data should be increased at large x by 1.4 (1.2) standard deviations of the dominant systematic errors. For both targets, one finds similar results for Λ and for the gluon distribution. A combined fit which is superimposed to the data in Fig. 4 gives

$$\Lambda^{(4)}_{\overline{MS}} = 263 \pm 42\,\text{MeV},$$

where the error indicates the total error; this result agrees with the fits to the BCDMS data only. For the gluon distribution which is parametrized as $xG(x, Q_0^2) = A(1+\eta)(1-x)^\eta$,

$$A = 0.40 \pm 0.07, \quad \eta = 5.5 \pm 1.5, \quad \text{at } Q_0^2 = 20\ \text{GeV}^2.$$

Note that the result on Λ corresponds to a measurement of α_s with an error of a few percent only, depending on the choice of Q^2; for example, it corresponds to

$$\alpha_s(M_Z^2) = 0.113 \pm 0.003$$

in excellent agreement with recent results from LEP [12]. The higher twist coefficients are shown in Fig. 5. The remarkable result here is that they are compatible with zero up to $x \approx 0.3$ when target mass corrections are included, indicating that purely perturbative QCD describes scaling violations in the small x regime down to Q^2 values below 1 GeV^2.

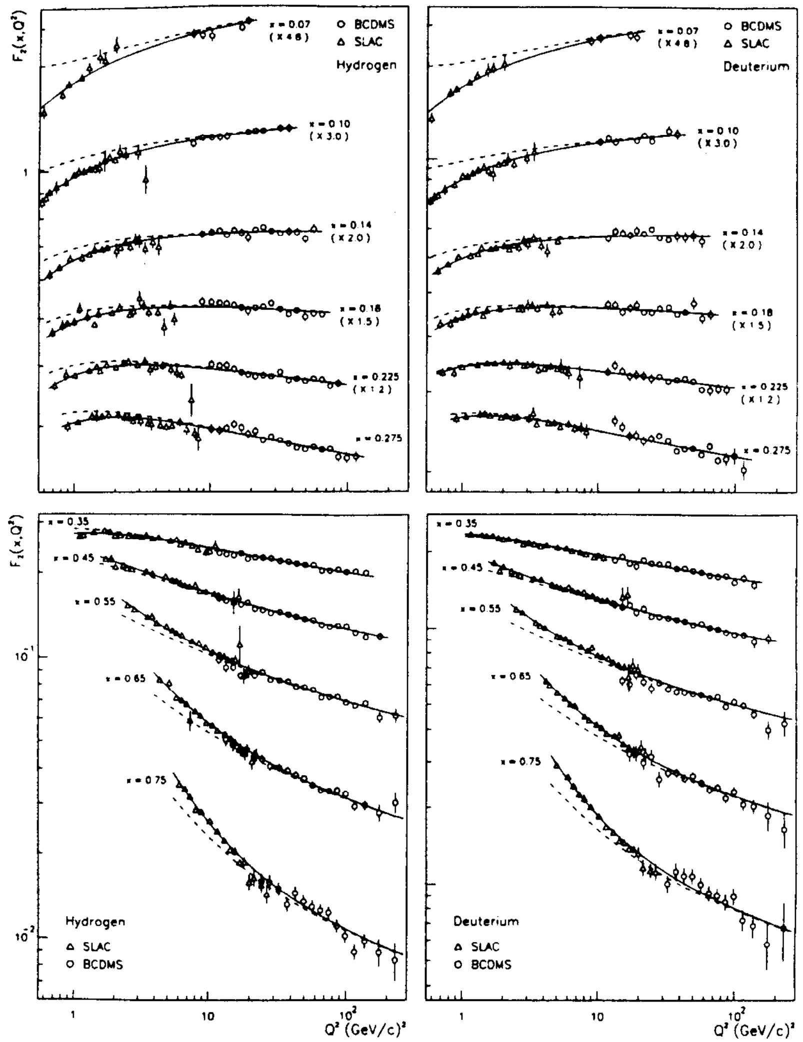

Figure 4: Next-to-leading order QCD fits to the combined SLAC and BCDMS data. The solid line is a fit including higher twist terms as described in the text; the dashed line shows the perturbative part F_2^{LT} only. Target mass corrections are included.

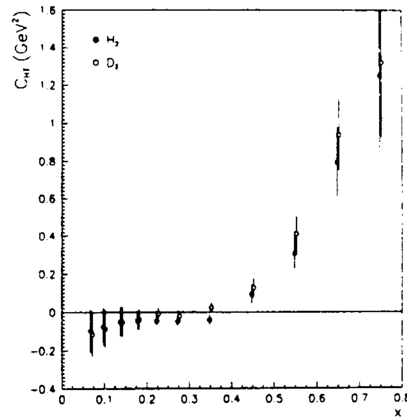

Figure 5: Higher twist coefficients from fits to the combined SLAC and BCDMS data as a function of x, for deuterium and hydrogen data.

The question of the "theoretical" uncertainty on α_s has recently received much attention, mostly in connection with experimental results on α_s from e^+e^- annihilation at LEP where the theoretical error is now the dominant one [12]. This uncertainty arises from the neglect of higher order terms in the QCD perturbation expansions, and is usually expressed in terms of a scale factor for the Q^2 appearing in the Altarelli-Parisi equations. When including such a scale uncertainty in their fits, Virchaux and Milsztajn find that the corresponding error on $\alpha_s(M_Z^2)$ is 0.004; combining experimental and theoretical uncertainties in quadrature, their final result on the strong coupling constant is

$$\alpha_s(M_Z^2) = 0.113 \pm 0.005.$$

In a similar study using a smaller, and partly different data set, Martin et al. have found [18]

$$\alpha_s(M_Z^2) = 0.109^{+0.007}_{-0.008},$$

in excellent agreement with ref. [16].

3 Measurements of spin structure functions

The physics of deep inelastic scattering with polarized high energy electron and muon beams is presently experiencing a Renaissance, following the seminal results obtained by the EMC on the spin structure function of the proton. The EMC result has raised a number of questions about the understanding of the dynamics of the nucleon spin at the parton level which have not been answered so far and

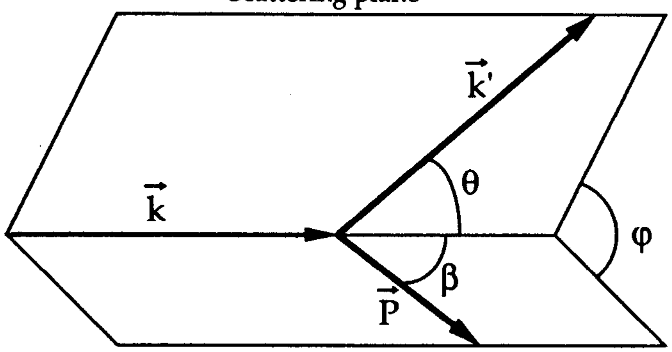

Figure 6: Kinematic planes of scattering of longitudinally polarized leptons.

will require more experimental information to be resolved theoretically, including data on the spin structure of the neutron which is totally unknown today.

3.1 Polarized lepton-nucleon scattering

A detailed account of the cross sections relevant for deep inelastic scattering of polarized leptons can be found in refs. [3, 19, 20, 21, 22]. The following brief review is limited to the phenomenology of the scattering of longitudinally polarized electrons and muons. The scattering of transversely polarized beams is not discussed here.

In the laboratory system, the scattering process is conveniently visualized in the two kinematic planes depicted in Fig. 6. The scattering plane is defined, as in the unpolarized case, by the momentum 3-vectors $\vec{k}$ and $\vec{k}'$ of the incoming and scattered lepton, respectively; θ is the scattering angle. The polarization plane is defined by $\vec{k}$ and by the polarization vector $\vec{P}$ of the nucleon. The angle between $\vec{k}$ and $\vec{P}$ is often referred to as β ($0 \leq \beta \leq \pi$) and ϕ is the angle between the scattering and the polarization planes.

The differential deep inelastic cross section for the process shown in Fig. 6 can be decomposed into an unpolarized piece σ_0 and a polarized piece $\Delta\sigma$,

$$\frac{d^3\sigma(\beta)}{dxdyd\phi} = \frac{d^3\sigma_0}{dxdyd\phi} - \frac{d^3\Delta\sigma(\beta)}{dxdyd\phi}. \tag{2}$$

In the Born approximation, the polarized piece is given by

$$\frac{d^3\Delta\sigma(\beta)}{dxdyd\phi} = \frac{2\alpha^2}{MExy}\Big\{\cos\beta\Big[\Big(1-\frac{y}{2}-\frac{Mxy}{2E}\Big)g_1(x,Q^2) - \frac{Mx}{2E}g_2(x,Q^2)\Big] -$$
$$\cos\phi\sin\beta\frac{\sqrt{Q^2}}{\nu}\Big(1-y-\frac{Mxy}{2E}\Big)^{\frac{1}{2}}\cdot\Big[\frac{y}{2}g_1(x,Q^2)+g_2(x,Q^2)\Big]\Big\}, \tag{3}$$

where g_1 and g_2 are the so-called spin structure functions of the nucleon. They play a central role in the understanding of the spin structure of nucleons.

An inspection of eq. (3) reveals immediately how these two structure functions can be disentangled experimentally from the measured differential cross section. For $\sin\beta = 0$, i.e., target polarization (anti)parallel to the beam direction, one mainly measures g_1 since g_2 is strongly suppressed at high energies by the factor $Mx/2E$. For $\cos\beta = 0$, i.e., transverse target polarization, g_1 and g_2 contribute to the measured cross section with approximately equal weight. So far, only the case of longitudinal target polarization has been studied experimentally and no data exist on g_2.

3.2 Spin structure functions in the Quark-Parton Model

The spin structure function g_1 has a straightforward interpretation in the QPM, similar to the unpolarized structure functions:

$$g_1(x) = \frac{1}{2}\sum_i e_i^2[q_i^+(x) - q_i^-(x)], \tag{4}$$

where $q_i^+(x)$ ($q_i^-(x)$) is the density of quarks with helicity parallel (antiparallel) to the nucleon spin. This interpretation of $g_1(x)$ can be understood from the fact that a virtual photon with spin projection +1 can only be absorbed by a quark with spin projection $-1/2$, and vice versa.

The interpretation of the "transverse" spin structure function g_2 in the QPM is much less obvious and is presently the subject of much theoretical debate [22]. Wandzura and Wilczek [23] have shown that in QCD it can be decomposed as

$$g_2(x,Q^2) = g_2^{WW}(x,Q^2) + \bar{g}_2(x,Q^2), \tag{5}$$

where the "trivial" piece g_2^{WW} is a "leading twist" (twist-2) contribution in the jargon of QCD, and is completely determined by $g_1(x,Q^2)$:

$$g_2^{WW}(x,Q^2) = -g_1(x,Q^2) + \int_x^1 \frac{dy}{y}g_1(y,Q^2). \tag{6}$$

The term $\bar{g}_2(x,Q^2)$ is a twist-3 contribution which seems to be best understood in an Operator Product Expansion (OPE) analysis in QCD, where it is sensitive to a quark-gluon correlation function in the nucleon and thus contains unique new physics. In Regge theory, g_2 is shown to fulfill, under certain conditions, the Burkhardt-Cottingham sum rule [24, 22]

$$\int_0^1 dx g_2(x, Q^2) = 0. \tag{7}$$

3.3 Sum rules for the spin structure function g_1

Just as for unpolarized structure functions, no theoretical predictions exist yet for the x dependence of their spin dependent counterparts, although such predictions are expected to emerge ultimately from non-perturbative QCD. Predictions do exist, however, in the form of sum rules related to polarized structure functions. The most general of these, and one of the most fundamental predictions of the QPM indeed, is the celebrated Bjorken sum rule [25]

$$\int_0^1 [g_1^p(x) - g_1^n(x)]dx = \frac{1}{6}\left|\frac{g_A}{g_V}\right|, \tag{8}$$

where p and n denote the proton and the neutron, respectively, and where g_A and g_V are the axial and vector weak coupling constants of nuclear beta decay. In this form, the sum rule was derived by Bjorken from light cone algebra and from very general assumptions on the partonic structure of the weak and electromagnetic hadronic currents. Nowadays, the sum rule (8) can be rigorously derived in QCD in the limit $Q^2 \to \infty$. At finite values of Q^2 [26],

$$\int_0^1 [g_1^p(x, Q^2) - g_1^n(x, Q^2)]dx = \frac{1}{6}\left|\frac{g_A}{g_V}\right|\left[1 - \frac{\alpha_s(Q^2)}{\pi}\right], \tag{9}$$

where α_s is the strong coupling constant.

Separate sum rules for the proton and the neutron were derived by Ellis and Jaffe for the proton and the neutron [27]. Ignoring QCD radiative corrections, they read

$$\int_0^1 g_1^p(x)dx = \frac{1}{12}\left|\frac{g_A}{g_V}\right|\left[+1 + \frac{5}{3}\frac{3F/D - 1}{F/D + 1}\right] \tag{10}$$

and

$$\int_0^1 g_1^n(x)dx = \frac{1}{12}\left|\frac{g_A}{g_V}\right|\left[-1 + \frac{5}{3}\frac{3F/D - 1}{F/D + 1}\right], \tag{11}$$

where F (D) are the antisymmetric (symmetric) $SU(3)$ couplings measurable in hyperon decays. These predictions are less fundamental than the Bjorken sum rule since they assume exact flavour $SU(3)$ symmetry of the baryon octet decays, and zero net polarization of the sea of strange quarks and heavier flavours.

No experimental data exist on g_1^n and the only sum rule which is tested experimentally until now is the Ellis-Jaffe prediction (10) for the proton. These data will be discussed in Sect. 3.5 below.

3.4 Cross section asymmetries

Since the polarized piece (3) gives, in general, only a small contribution to the experimentally measured cross section, it is customary to evaluate it from measurements of cross section asymmetries in which the unpolarized part cancels. In the most simple case where both the beam and the target are longitudinally polarized (i.e., $\sin\beta = 0$), this asymmetry is

$$A = \frac{\sigma^{\uparrow\downarrow} - \sigma^{\uparrow\uparrow}}{\sigma^{\uparrow\downarrow} + \sigma^{\uparrow\uparrow}} \tag{12}$$

where $\sigma^{\uparrow\downarrow}$ and $\sigma^{\uparrow\uparrow}$ are the cross sections for opposite and equal spin directions, respectively. From equations (2)–(4), neglecting terms of order M/E, one finds

$$A = D[A_1 + \eta A_2], \tag{13}$$

where

$$A_1(x) = \frac{g_1(x)}{F_1(x)} = \frac{\sum_i e_i^2[q_i^+(x) - q_i^-(x)]}{\sum_i e_i^2[q_i^+(x) + q_i^-(x)]}, \tag{14}$$

$$A_2(x) = \sqrt{\frac{2Mx}{Ey}}\frac{g_1(x) + g_2(x)}{F_1(x)}. \tag{15}$$

D is sometimes called the depolarization factor of the virtual photon and is given by

$$D = \frac{2y - y^2}{2(1-y)(1+R) + y^2}; \tag{16}$$

the factor η depends only on kinematic variables:

$$\eta = \frac{\sqrt{Q^2}}{E}\frac{2(1-y)}{y(2-y)}. \tag{17}$$

A_1 and A_2 can also be interpreted as virtual photon-nucleon asymmetries

$$A_1 = \frac{\sigma_{1/2} - \sigma_{3/2}}{\sigma_{1/2} + \sigma_{3/2}}, \tag{18}$$

$$A_2 = \frac{2\sigma_{TL}}{\sigma_{1/2} + \sigma_{3/2}}, \tag{19}$$

where 1/2 and 3/2 are the total spin projections in the direction of the virtual photon, and σ_{TL} is a cross section arising from the interference of amplitudes for longitudinal and transverse polarized virtual photons. The following bounds can be derived for A_1 and A_2 [28]:

$$|A_1| \leq 1, \qquad |A_2| \leq R; \tag{20}$$

for this reason, A_2 is expected to give a small contribution to A and is usually ignored.

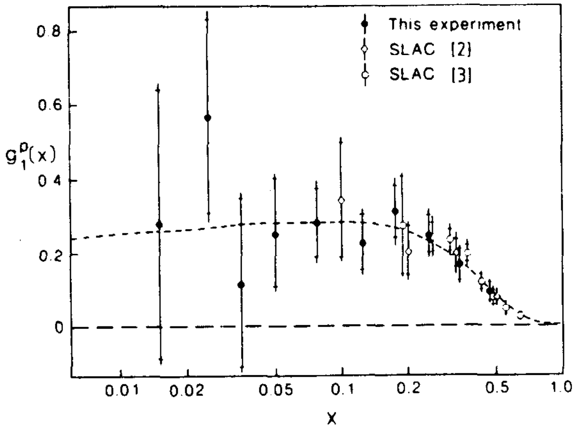

Figure 7: The spin structure function $g_1^p(x)$ measured by the EMC ("This experiment") and the SLAC-Yale collaborations. The dashed curve is a phenomenological parametrisation.

Finally, the experimentally measured counting rate asymmetry is related to the cross section asymmetry (12) by

$$A_{exp} = f_t P_t P_\mu A, \tag{21}$$

where P_μ is the beam polarization, P_t the polarization of the target nucleons, and f_t the target dilution factor, i.e., the fraction of polarized nucleons in the target material.

3.5 The proton spin crisis

The most recent data on spin structure functions were presented in 1987 by the EMC [29, 30]. The EMC measurement of $g_1^p(x)$ was found to be in good agreement with earlier data from the SLAC-Yale experiments [31] but covers a significantly larger kinematic range in the x variable (Fig. 7). These data therefore allowed the first significant test of the Ellis-Jaffe sum rule which is shown in Fig. 8.

Using the parametrisation of Fig. 7 to extrapolate the measured integral to $x = 0$, the result from the combined EMC and SLAC data is

$$\int_0^1 g_1^p(x)dx = 0.126 \pm 0.010\,(\text{stat.}) \pm 0.015\,(\text{syst.}).$$

The Ellis-Jaffe prediction, using the most recent data on F/D [32], is

$$\int_0^1 g_1^p(x)dx = 0.189 \pm 0.005,$$

i.e., there is a 3.5 standard deviation discrepancy between the Ellis-Jaffe prediction and the experimental data.

The quark contribution to the total spin of the proton is given by

$$\frac{1}{2}\Delta\Sigma = \frac{1}{2}(\Delta u + \Delta d + \Delta s) \tag{22}$$

where heavier flavours have been neglected and where

$$\Delta q = \int_0^1 [q^+(x) + \bar{q}^+(x) + q^-(x) + \bar{q}^-(x)] \tag{23}$$

is, apart from a factor 1/2, the contribution to the nucleon spin from an individual quark flavour. Using a generalization of the Ellis-Jaffe sum rule by Glück and Reya which includes QCD radiative corrections [33], assuming isospin invariance and the same experimental data on the $SU(3)$ couplings F and D, it can be shown that [30]

$$\frac{1}{2}\Delta\Sigma = 0.060 \pm 0.047\,(\text{stat.}) \pm 0.069\,(\text{syst.}),$$

i.e., the quark contribution to the total proton spin is compatible with zero within the experimental errors. The proton spin fulfills the sum rule

$$S_p = \frac{1}{2} = \frac{1}{2}\Delta\Sigma + \frac{1}{2}\Delta g + < L_z >, \tag{24}$$

where Δg is the gluon equivalent of $\Delta\Sigma$ and $< L_z >$ is the mean z component of the orbital angular momentum of the partons. Most of the proton spin must therefore be carried by gluons and/or parton orbital momentum. This surprising result has triggered intense theoretical efforts to explain the spin composition of the proton. The recent literature on this subject is too vast to be reviewed here [34].

3.6 New experiments on spin dependent structure functions

Following the unexpected result of the EMC experiment, several new experiments to study spin dependent structure functions have been proposed, most of which share the following main goals:

- New measurements of $g_1^p(x)$ for an improved test of the Ellis-Jaffe sum rule for the proton,

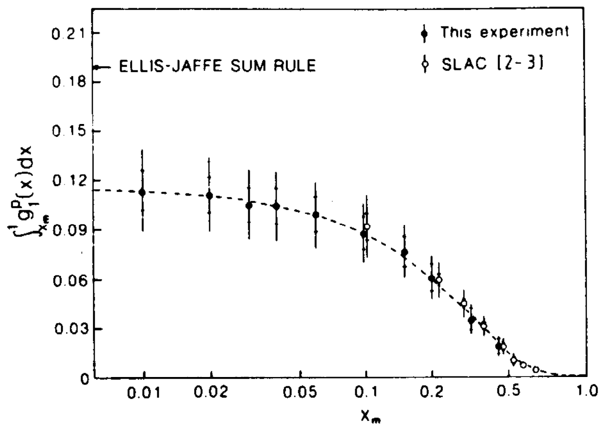

Figure 8: The integral $\int_{x_m}^{1} g_1^p(x)dx$ as a function of the lower integration limit x_m. The prediction of the Ellis-Jaffe sum rule is also shown.

- measurement of the neutron distribution $g_1^n(x)$ and test of the corresponding Ellis-Jaffe sum rule,
- test of the Bjorken sum rule,
- measurement of the "transverse" spin structure function $g_2(x)$.

The study of other related physical questions has also been proposed by several of these next generation experiments [35].

The direct successor of the EMC is the SMC experiment which has recently started to take data at CERN. All other experiments which are presently proposed or in preparation use polarized electron beams.

3.7 The SMC experiment

The SMC (Spin Muon Collaboration) experiment [36] uses an upgraded configuration of the apparatus built for the earlier EMC experiments [1, 29, 30]. The experiment makes use of the fact that high energy muon beams produced by decay of pions and Kaons in flight are naturally polarized due to parity violation [37]. Polarizations of about 80% are easily obtained with the CERN muon beam.

The high energy muons are scattered off two solid targets polarized in opposite directions. The target materials are deuterated and normal hydrocarbon glasses, doped with a small amount of paramagnetic metallo-organic substance EHBA-Cr(V) or its deuterated version. The glass matrix consists mainly of 1-butanol C_4H_9OH(95%) and water (5%), or their deuterated forms. The dilution factors for free hydrogen (deuterium) nuclei in these materials are $f_p = 0.13$ and $f_d = 0.23$.

The Dynamic Nuclear Polarization (DNP) [38] technique is used to obtain high nuclear polarizations in the targets. In this technique the paramagnetic electron spin system in the material is saturated slightly off-resonance (70 GHz); this produces dynamic cooling of the spin-spin interactions among the electrons by a factor around $\pm 1/400$. The nuclear spins are cooled to a temperature very close to that of the electron spin-spin interactions, because no other thermal contact to the nuclear spin system is provided in the material. If the material is cooled to 500 mK by a $^3He - ^4He$ dilution refrigerator, nuclear spin temperatures around ± 2 mK can be obtained.

The target material is arranged inside a superconducting solenoid, with a 2.5 Tesla field of high homogeneity, in two cells so that each cell can be irradiated with microwave power from an independent source. The microwave frequencies are adjusted just below and just above the electron spin resonance line so that maximum positive and negative polarizations are obtained in the two target cells. In the present materials the proton polarizations of $\pm 85\%$ and deuteron polarizations of about $\pm 30\%$ have been obtained in the large target cells containing each about 500 g of solid target material.

The target is cooled with a powerful dilution refrigerator [39] so that the microwave losses of about 2 W in the material can be cooled at a helium temperature of 0.5 K. When the microwave power is turned off, the refrigerator cools the material to about 50 mK temperature, where the nuclear spin lattice relaxation becomes extremely slow, thus enabling the "freezing" of the target polarization. The polarization of such a frozen-spin target is insensitive to the magnetic field inhomogeneity, and reasonably slow relaxation is measured down to 0.5 Tesla field value. In this mode the target polarizations can be reversed by the rotation of the magnetic field, which is accomplished by exciting a dipole magnet superimposed on the solenoid, while ramping the solenoid current through zero value.

The target polarization is measured with $\pm 3\%$ relative accuracy by continuous wave NMR techniques using a series-resonant circuit and a Q-meter with real-part detector. The polarization can also be monitored continuously during frozen-spin operation in 0.5 T field.

During a first phase (1991/92), the SMC uses an improved version of the target set-up which was originally built for the EMC experiment [40]. From 1993 onwards, a new target configuration will be used with longer target cells (60 cm instead of 36 cm each) in a bigger cryostat, a new solenoid with improved field homogeneity for higher polarization, and a more powerful refrigerator. In this configuration, a transverse dipole field can be superimposed to the solenoid field which is employed for fast polarization reversal by field rotation in frozen spin mode, or for tranverse target polarization to measure g_2. It is expected that a proton polarization of more than 80% and deuteron polarizations of up to 40% will be achieved with this target.

The muon spectrometer of the SMC experiment is an upgraded version of the well-known EMC apparatus (Fig. 9). A high precision measurement of the scattering angle and of the momentum of charged particles is provided by a large aperture dipole magnet ($\int B\,dl$ = 2.3 Tm) instrumented with multiwire proportional chambers and drift chambers. The momentum measurement stage is followed by a muon identification stage which consists of an iron absorber to remove the hadrons produced in the deep inelastic interaction, an array of large-surface streamer tubes and drift tubes to measure the muon tracks behind the absorber, and two arrays of scintillator hodoscopes which provide the muon trigger of the experiment.

The muon spectrometer is followed by a beam polarimeter [36] which has been newly designed for the SMC experiment. With this apparatus, the beam polarization is determined mainly by measuring the energy spectrum of electron or positrons from muon decay in flight. It provides a 30 m long decay space for the muons, the beginning of which is defined by an electromagnetic shower counter to suppress background from electromagnetic interactions in material exposed to the upstream beam. Decay electrons are identified and momentum analyzed by a simultaneous measurement of their momentum and energy in a magnetic spectrometer and in a lead-glass calorimeter. A magnetized iron target for polarization measurement with the Møller scattering method is also under construction.

The SMC experiment will test the sum rules (9)–(11) to an accuracy of 10–20% which will be dominated by systematic errors. The main uncertainties are the measurement errors on the beam and target polarization and the uncertainty in the extrapolation of $g_1(x)$ to $x = 0$.

3.8 Electron beam experiments

Four experiments are presently under construction, or have been proposed, to study spin structure functions in polarized electron beams:

- The SLAC E-142 experiment [41] which has been approved and is scheduled to take data in the fall of 1992;
- The SLAC E-143 experiment [42], which has also been approved and is scheduled to take data in 1993;
- The HERMES experiment [43] proposed for the high intensity internal electron beam of the HERA electron-proton storage ring at DESY;
- The HELP experiment [44] proposed for the polarized internal 45 GeV beam of the LEP electron-positron storage ring at CERN.

A detailed discussion of most of the experiments listed here can be found in ref. [35].

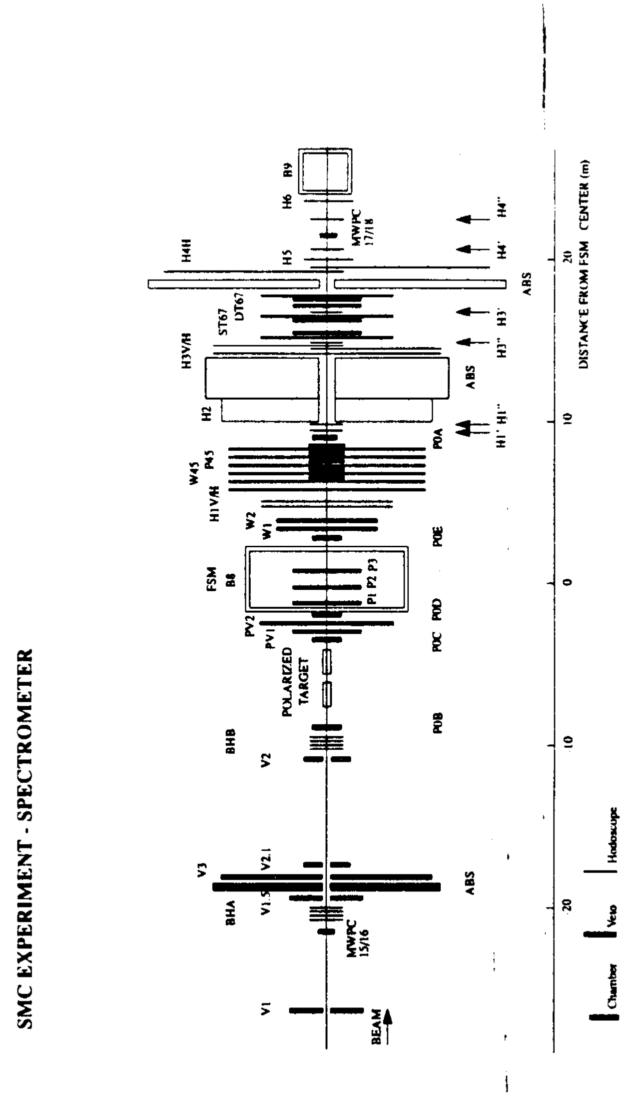

Figure 9: Schematic layout of the SMC spectrometer. The muon beam arrives from the left and impinges on a twin solid state target. Downstream of the target, one distinguishes the momentum measurement stage with the Forward Spectrometer Magnet (FSM), and the muon identification system downstream of the absorber (ABS). The detectors to the left of the target are beam defining counters to measure the track of the incident muon, and veto counters to shield the experiment from halo muons.

4 Conclusion

Deep inelastic scattering experiments continue making significant progress towards a better, and ever more detailed, understanding of the quark structure of matter. Recent progress in charged lepton scattering has been mainly in the area of measurements on free nucleon targets, where electron and muon data now complement each other to form an impressive set of data covering more than two orders of magnitude in four-momentum transfer; some experimental discrepancies are beginning to fade away. The combined electron and muon data also serve as a base of what is probably the most significant and precise test of QCD from scaling violations performed so far, providing at the same time a significant measurement of Λ_{QCD} and of the strong coupling constant.

The EMC results on the spin structure function of the proton have resuscitated a major interest in the experimental and theoretical study of the internal spin structure of hadrons. A new generation of experiments, exploiting a large variety of different techniques for spectrometers and beam and target polarization, has recently started to collect data. In about five years from now our understanding of spin structure functions, which is scarce and incomplete today, should have substantially improved.

References

[1] EMC, O.C. Allkofer et al., Nucl. Instr. Meth. 179 (1981) 445; J.P. Albanese et al., Nucl. Instr. Meth. 212 (1983) 111.

[2] BCDMS, D. Bollini et al., Nucl. Instr. Meth. 204 (1983) 333; A.C. Benvenuti et al., Nucl. Instr. Meth. 226 (1984) 330.

[3] T. Sloan, G. Smadja and R. Voss, Phys. Rep. 162 (1988) 45.

[4] BCDMS, A.C. Benvenuti et al., Phys. Lett. B223 (1989) 485.

[5] BCDMS, A.C. Benvenuti et al., Phys. Lett. B237 (1989) 592.

[6] EMC, J.J. Aubert et al., Nucl. Phys. B259 (1985) 189.

[7] EMC, J.J. Aubert et al., Nucl. Phys. B239 (1987) 740.

[8] A. Milsztajn et al., Z. Phys. C 49 (1991) 527.

[9] L.W. Whitlow, Ph.D. Thesis, Stanford University, SLAC-Report-357, March 1990.

[10] I.G. Bird, Proc. 1991 Joint Int. Symp. on Lepton-Photon Interactions and Europhysics Conf. on High Energy Physics (LP-HEP'91), Geneva, World Scientific, in print.

[11] S.R. Mishra, Proc. 1991 Joint Int. Symp. on Lepton-Photon Interactions and Europhysics Conf. on High Energy Physics (LP-HEP'91), Geneva, World Scientific, in print; S.R. Mishra, these proceedings.

[12] T. Hansl, these proceedings.

[13] G. Altarelli and G. Parisi, Nucl. Phys. B126 (1977) 298.

[14] BCDMS, A.C. Benvenuti et al., Phys. Lett. B195 (1987) 97.

[15] BCDMS, A.C. Benvenuti et al., Phys. Lett. B223 (1989) 490.

[16] M. Virchaux and A. Milsztajn, Phys. Lett. B274 (1992) 221.

[17] H. Georgi and D. Politzer, Phys. Rev. D14 (1976) 1829.

[18] A.D. Martin, R.G. Roberts and W.J. Stirling, Phys. Rev. D43 (1991) 3648; Phys. Lett. B266 (1991) 273.

[19] T. Kamae, Y. Shimiziu and M. Igarashi, eds., Report of the TRISTAN ep (ee) Working Group, University of Tokyo preprint UTPN-165 (UT-345) (1980).

[20] N.S. Craigie et al., Phys. Rep. 99 (1983) 69.

[21] V.W. Hughes and J. Kuti, Ann. Rev. Nucl. Part. Sci. 33 (1983) 611.

[22] R.L. Jaffe, Comments Nucl. Part. Phys. 19 (1990) 239.

[23] S. Wandzura and F. Wilczek, Phys. Lett. 72B (1977) 195.

[24] H. Burkhardt and W.N. Cottingham, Ann. Phys. (N.Y.) 56 (1970) 453.

[25] J.D. Bjorken, Phys. Rev. 148 (1966) 1467; Phys. Rev. D1 (1970) 465; ibid. D1 (1970) 1376.

[26] J. Kodaira et al., Phys. Rev. D20 (1979) 627.

[27] J. Ellis and R.L. Jaffe, Phys. Rev. D9 (1974) 1444; D10 (1974) 1669.

[28] M.G. Doncel and E. de Rafael, Nuovo Cimento 4A (1971) 363; P. Gnădig and F. Niedermayer, Nucl. Phys. B55 (1973) 612.

[29] EMC, J. Ashman et al., Phys. Lett. 206B (1988) 364.

[30] EMC, J. Ashman et al., Nucl. Phys. B328 (1989) 1.

[31] SLAC-Yale E80 Collaboration, M.J. Alguard et al., Phys. Rev. Lett. 37 (1976) 1261; ibid. 41 (1978) 70; SLAC-Yale E180 Collaboration, G. Baum et al., Phys. Rev. Lett. 51 (1983) 1135; SLAC-Yale Collaboration, G. Baum et al., Phys. Rev. Lett. 45 (1980) 2000.

[32] M. Bourquin et al., Z. Phys. C21 (1983) 27.

[33] M. Glück und E. Reya, Z. Phys. C39 (1988) 569.

[34] For recent reviews see e.g.: H. Rollnik, Proc. 9th Int. Symp. on High Energy Spin Physics, Bonn 1990, K.-H. Althoff and W. Meyer, eds., p. 183; E. Reya, Dortmund preprint DO-TH 91/09.

[35] K. Rith, Proc. 9th Int. Symp. on High Energy Spin Physics, Bonn 1990, K.-H. Althoff and W. Meyer, eds., p. 198.

[36] The Spin Muon Collaboration (SMC), Measurement of the spin-dependent structure functions of the neutron and proton, CERN/SPSC 88-47 (SPSC/P242), 1988.

[37] L.M. Lederman and M.J. Tannenbaum, Advances in Particle Physics, Vol. I, New York 1968, p. 11.

[38] M. Borghini, Phys. Rev. Lett. 20 (1968) 419.

[39] T.O. Niinikoski, Nucl. Instr. and Meth. 192 (1982) 151.

[40] S.C. Brown et al., in Proc. Proc. 4th Workshop on Polarized Target Materials and Techniques, Bonn 1984, ed. W. Meyer, (Physikalisches Institut, Universität Bonn, Bonn 1984) p. 102.

[41] R. Arnold et al., A proposal to measure the neutron spin dependent structure function, SLAC Proposal E-142, 1989.

[42] E143 Collaboration, R. Arnold et al., Measurements of the Nucleon Spin structure at SLAC in End Station A.

[43] The HERMES Collaboration, A Proposal to Measure the Spin-Dependent Structure Functions of the Neutron and the Proton at HERA, DESY-PRC 90/01, 1990.

[44] G. Ballocchi et al., CERN/LEPC 89-10, (LEPC/M 88), 1989.